Validity of the generalized density matrix method for the microscopic calculation of a collective/bosonic Hamiltonian

L. Y. Jia (贾力源)* and V. G. Zelevinsky
National Superconducting Cyclotron Laboratory and Department of Physics and Astronomy, Michigan State University, East Lansing, Michigan 48824, USA
(Received 14 May 2012; published 16 July 2012)

Recently a generalized density matrix (GDM) procedure was proposed [Jia and Zelevinsky, Phys. Rev. C **84**, 064311 (2011)] for calculating a collective/bosonic Hamiltonian microscopically from the shell-model Hamiltonian. In this work we examine the validity of the method by comparing the GDM results with those of the exact shell-model diagonalization in a number of models. It is shown that the GDM method reproduces the low-lying collective states quite well, both for energies and transition rates, across the whole region going from vibrational to γ-unstable and deformed nuclei.

DOI: 10.1103/PhysRevC.86.014315 PACS number(s): 21.60.Ev, 21.10.Re

I. INTRODUCTION

A long-standing problem in nuclear physics is understanding how macroscopic collective dynamics arise from microscopic single-particle motion. The shell model (configuration interaction) successfully reproduces various collective behaviors by diagonalizing the nucleonic Hamiltonian in a huge Slater-determinant basis. However, the dimension of the basis makes it impractical for cases with many relevant orbitals. On the other hand, phenomenological bosonic approaches are often successful in explaining the experimental data (first of all the geometric Bohr Hamiltonian [1,2] and the interacting boson model [3]). This shows that, out of the huge Slater-determinant space, there exist a few collective degrees of freedom, which are usually sufficient for describing the low-lying collective states. Serious efforts were devoted to deriving the parameters of the collective Hamiltonian from the underlying shell-model Hamiltonian. However, the complete theory is still missing.

Recently we proposed [4] a procedure based on the generalized density matrix (GDM) that was originally formulated in Refs. [5–8]. This procedure is simple, clean, and consistent. In compact form, there are only two equations, Eqs. (14) and (23) in Ref. [4]. Results from the lowest orders give the well-known Hatree-Fock (HF) equations and random phase approximation (RPA). Higher orders fix the anharmonic terms in the collective/bosonic Hamiltonian. The aim of this work is to demonstrate the validity of the GDM method. In the next section we compare the GDM results with those of the exact shell-model diagonalization in a number of models.

II. COMPARISON WITH EXACT RESULTS

In this work, for simplicity, we restrict ourselves to systems without rotational symmetry. The GDM formulation with angular-momentum vector coupling has been considered in Ref. [9]. The single particle (s.p.) space in this work is drawn schematically in Fig. 1. There are two groups of degenerate s.p. levels. The Fermi surface is in between; thus without interaction, the lower levels are completely filled and upper levels are empty. Each s.p. level has a quantum number m that is a half integer. Degenerate time-reversal pairs have m of opposite sign, $m_{\bar{1}} = -m_1$. For fermions, $|\tilde{\tilde{1}}\rangle = -|1\rangle$, and we choose the phases such that

$$|\widetilde{m}\rangle = |-m\rangle, |\widetilde{-m}\rangle = -|m\rangle \ (m > 0).$$

We assume a two-body Hamiltonian,

$$H = \sum_1 e_1 a_1^\dagger a_1 + \frac{1}{4}\sum_{1234} V_{1234} N[a_1^\dagger a_2^\dagger a_3 a_4], \qquad (1)$$

where the s.p. energies $e_1 = \pm\frac{1}{2}$ for the upper and lower levels, respectively. The density matrix without interaction is $\rho_{12} = \delta_{12} n_1$, where the occupation number $n_1 = 1(0)$ for the lower (upper) s.p. levels. $N[a_1^\dagger a_2^\dagger a_3 a_4]$ is the normal-ordering form of operators. The residual interaction is of multipole-multipole type,

$$V_{1234} = -\kappa(q_{14}q_{23} - q_{13}q_{24}),$$

where the multipole operator $Q = \sum_{12} q_{12} a_1^\dagger a_2$ is Hermitian and time even. For simplicity we assume that q is real, and thus

$$q_{12} = q_{21} = q_{\bar{2}\bar{1}} = q_{\bar{1}\bar{2}}.$$

Operator q has certain selection rules with respect to quantum number m, which will be specified later. We further set diagonal matrix elements of q to zero, $q_{11} = 0$; hence in the mean field, $Q^{(00)} = \mathrm{Tr}[q\rho] = 0$.

Following the procedure in Ref. [4], we are able to map the fermionic Hamiltonian (1) onto a bosonic Hamiltonian,

$$H_b = \omega^2\frac{\alpha^2}{2} + \frac{\pi^2}{2} + \Lambda^{(30)}\frac{\alpha^3}{3!} + \Lambda^{(12)}\frac{\{\alpha,\pi^2\}}{4} + \Lambda^{(40)}\frac{\alpha^4}{4!} + \Lambda^{(22)}\frac{\{\alpha^2,\pi^2\}}{8} + \Lambda^{(04)}\frac{\pi^4}{4!} + \Lambda^{(50)}\frac{\alpha^5}{5!} + \cdots, \qquad (2)$$

where the collective coordinate α and momentum π satisfy $[\alpha,\pi] = i$. Together, the generalized density matrices $r^{(mn)}$

*jial@nscl.msu.edu

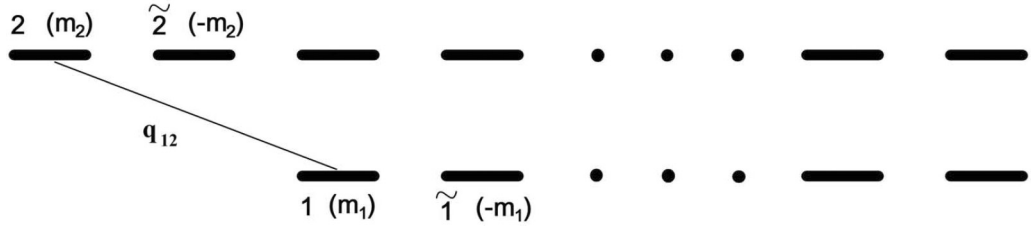

FIG. 1. Single-particle level scheme. $\tilde{1}$ is the time-reversal level of 1. Each level has a quantum number m.

defined in the expansion

$$R_{12} \equiv a_2^\dagger a_1 = \rho_{12} + r_{12}^{(10)}\alpha + r_{12}^{(01)}\pi + r_{12}^{(20)}\frac{\alpha^2}{2} + \cdots \quad (3)$$

are solved in terms of $\Lambda^{(mn)}$. The bosonic Hamiltonian H_b (2) should reproduce the low-lying collective spectrum of the original nucleonic Hamiltonian H (1). Substituting the solution (3) into $Q = \sum_{12} q_{12} a_1^\dagger a_2$, we get the boson image of the multipole operator,

$$Q_b = Q^{(10)}\alpha + Q^{(20)}\frac{\alpha^2}{2} + Q^{(02)}\frac{\pi^2}{2} + Q^{(30)}\frac{\alpha^3}{3!} + \cdots, \quad (4)$$

where $Q^{(mn)} = \mathrm{Tr}[q r^{(mn)}]$, and time-odd terms vanish automatically. The transition rates calculated from Q_b between eigenstates of H_b should reproduce those of Q between eigenstates of H.

As shown in Ref. [4], the GDM method fixes H_b completely. In each even order (quadratic, quartic,...) in H_b, the GDM method gives one constraint on $\Lambda^{(mn)}$'s. The number of constraints is the same as that of independent parameters in H_b, removing in Eq. (2) superficial degrees of freedom owing to canonical transformations of α and π conserving $[\alpha, \pi] = i$.

In the following we consider four models with different structures (different configurations of s.p. levels and different selection rules of q).

Model 1. We start with the simplest case. Both the upper and lower group have 12 degenerate s.p. levels with quantum numbers $m = \pm\frac{1}{2}, \pm\frac{3}{2}, \ldots, \pm\frac{11}{2}$. Operator q has the selection rule $\Delta m = 0$; that is, q_{12} vanishes unless $m_1 = m_2$. The nonvanishing matrix elements q_{12} $(m_1 = m_2)$ are set to be 1.

In this model we find by numerical computation an additional "symmetry." Namely, in Hamiltonian (2) there are only three nonvanishing terms: ω^2, $\Lambda^{(40)}$, and $\Lambda^{(22)}$ (besides $\pi^2/2$). This is similar to the "quasi-angular-momentum symmetry" in the Lipkin model, where the only three nonvanishing terms are ω^2, $\Lambda^{(40)}$, and $\Lambda^{(04)}$ (see Ref. [4]).

The results for this model are shown in Fig. 2. The GDM calculation reproduces the exact results of the shell model quite well, both for energies and transition rates. In the shell model we calculate the lowest several states by the Lanczos method. The dashed line in the upper panel is the beginning of the s.p. continuum (s.p. excitations with high level density); only those collective states below the continuum are calculated (due to computation time). In the GDM calculation the resulting bosonic Hamiltonian is diagonalized in a finite "physical" bosonic space, $\{|0 \leqslant n \leqslant 12\rangle\}$, where 12 is the number of fermions. $|n\rangle$ is the n-phonon state, $A^\dagger A|n\rangle = n|n\rangle$, and $A^\dagger = (u\alpha + iv\pi)/\sqrt{2}$, $uv = -1$. The coefficient u is fixed by minimizing $A|\mathrm{HF}\rangle$ in its one-particle–one-hole components, where $|\mathrm{HF}\rangle$ is the Hartree-Fock ground state that is mapped onto the bosonic state $|n = 0\rangle$. The result is $u^4 = \frac{\sum_{2<F<1}|r_{12}^{(10)}|^2}{\sum_{2<F<1}|r_{12}^{(01)}|^2}$, where the summation indices 1 and 2 run over unoccupied and occupied s.p. levels, respectively (F denotes Fermi surface). In models of this work, u is a number close to 1. The shown GDM energies and transitions are practically independent of small variations of u around the above value.

As κ increases, the system goes from vibrational to γ-unstable region. In the vibrational region, higher excited states are influenced more by the anharmonicities, as expected. At large κ the spectrum becomes doubly degenerate in a deep double-well potential (large negative ω^2). This is the analog of γ-instability of realistic nuclei in three dimensions.

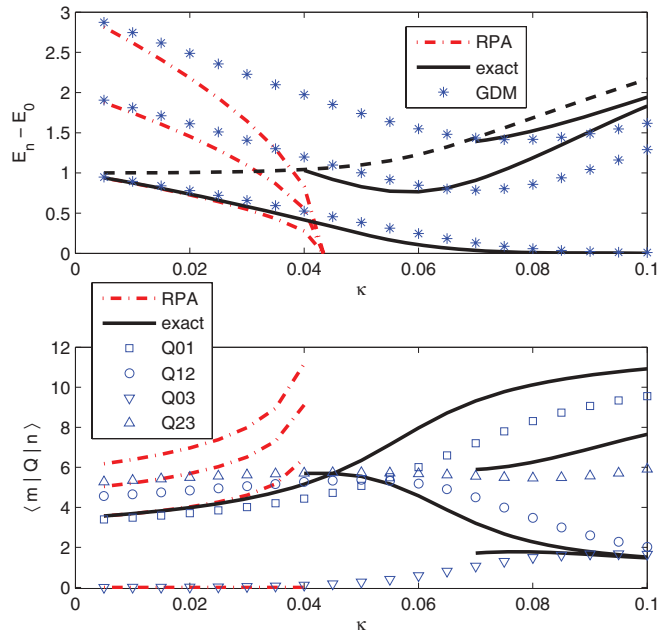

FIG. 2. (Color online) Excitation energies $E_n - E_0$ and transition matrix elements $\langle m|Q|n\rangle$ in model 1 as a function of κ. The black solid lines are exact results of shell-model diagonalization. The black dashed line is the beginning of the single-particle continuum. The red dashed-dotted lines are the RPA results. The blue symbols are the GDM results. The stars are energies; the squares, circles, up triangles, and down triangles are matrix elements of Q between different states. Matrix elements $\langle m|Q|n\rangle$ that are not shown vanish in both the shell model and the GDM calculations.

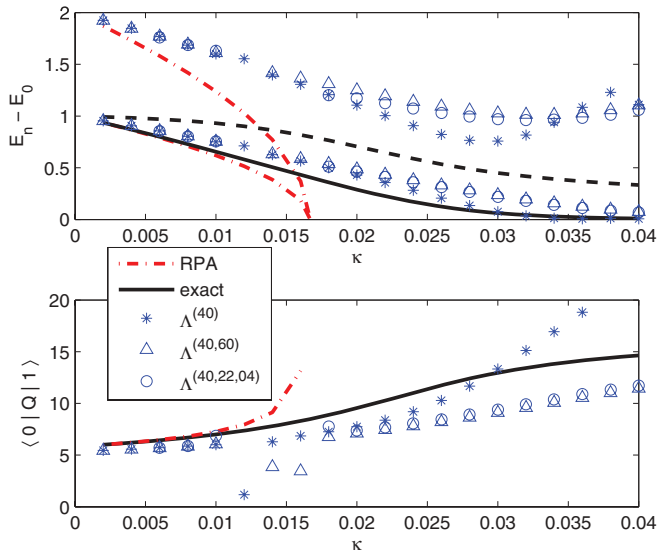

FIG. 3. (Color online) Excitation energies $E_n - E_0$ and transition matrix elements $\langle 0|Q|1\rangle$ in model 2 as a function of κ. The black solid lines are exact results of shell-model diagonalization. The black dashed line is the beginning of the single-particle continuum. The red dashed-dotted lines are the RPA results. The blue symbols (stars, up triangles, and circles) are results of three different sets of GDM calculations, as labeled in the legend.

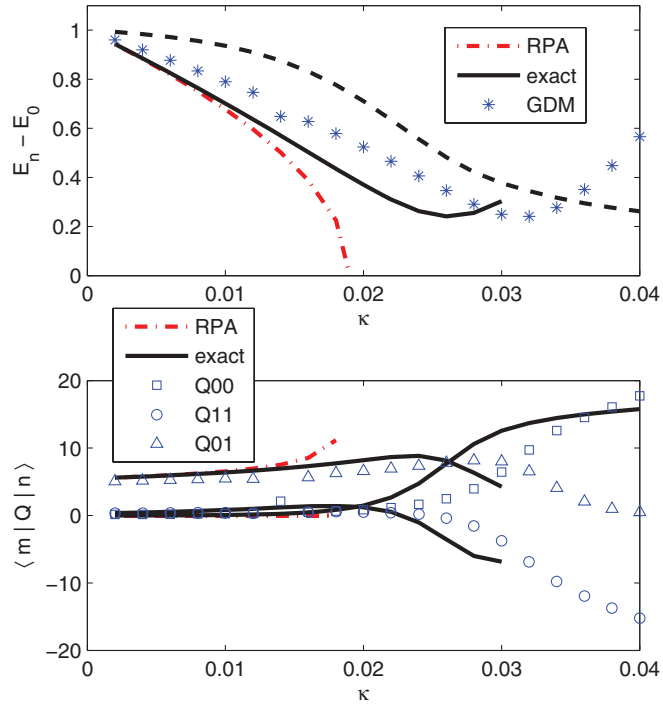

FIG. 4. (Color online) Excitation energies $E_n - E_0$ and transition matrix elements $\langle m|Q|n\rangle$ in model 3 as a function of κ. The black solid lines are exact results of shell-model diagonalization. The black dashed line is the beginning of the single-particle continuum. The red dashed-dotted lines are the RPA results. The blue symbols are the GDM results. The stars are energies; the squares, circles, and up triangles are matrix elements of Q between different states.

An important point is that the GDM method works better with increasing collectivity Ω, the number of effective simple particle-hole excitations contributing to the collective mode. Another calculation has been done (not shown here) with 8 particles in 16 s.p. levels. The GDM results of the current calculation (12 particles in 24 s.p. levels) have very clear improvement over those of the former. In other words, the error in Fig. 2 may be of order $1/\Omega$. The largest part of this error may come from the RPA frequency ω^2. At the current stage, the GDM method calculates all $\Lambda^{(mn)}$ in their leading order of $1/\Omega$ but not the next. If the correct $\omega^2 = \Lambda^{(20)}$ was smaller by a $1/\Omega$ term than the one determined here by the RPA equation, all the GDM curves would be shifted to the left (smaller κ), which would decrease greatly the systematic error (see Fig. 2). This systematic error owing to inaccurate ω^2 was present in all models in this work (see Figs. 3–5). Also, it is confirmed in the Lipkin model where everything is known analytically (see Ref. [4]). Hence an achieved improvement would be calculating ω^2 in its next-to-leading order of $1/\Omega$.

Model 2. This model has the same s.p. configuration, but the operator q has now the selection rule $\Delta m = 0, \pm 1$. Nonvanishing q_{12} are still set to be 1. Here we do not find additional symmetry as in model 1, so the problem exists of what should be the "best" mapping. In the following we did three sets of GDM calculations. The first calculation is possibly simplest, which keeps only $\Lambda^{(40)}$ (besides $\omega^2\alpha^2/2$ and $\pi^2/2$) in H_b, fixed by the constraint from the fourth order in equation of motion (EOM). The second calculation keeps the lowest two potential (no π dependence) terms $\Lambda^{(40)}$ and $\Lambda^{(60)}$, which are fixed by the two constraints from up to the sixth order in EOM. The third calculation keeps all quartic anharmonicities, $\Lambda^{(40)}$, $\Lambda^{(22)}$, and $\Lambda^{(04)}$, fixed by the three constraints from up to the eighth order in EOM.

We first notice in Fig. 3 that in this model the s.p. continuum goes down with increasing κ, as opposed to going up in model 1. This is because now mixing of s.p. levels within the upper (lower) group is allowed by the selection rule that Δm can be ± 1. As a result, originally degenerate levels from the upper (lower) group get a finite spread, which reduces the gap of the s.p. continuum. Only the first excited state is within the gap and calculated in the shell model.

In the GDM calculations we see that the simplest one-degree-of-freedom ($\Lambda^{(40)}$) calculation is reasonably good in most cases except at very large κ. The other two calculations ($\Lambda^{(40/60)}$ and $\Lambda^{(40/22/04)}$) give essentially the same results (for the quantities shown in Fig. 3), although their common parameter, $\Lambda^{(40)}$, is different. This insensitivity of GDM results to the degrees of freedom chosen, is important. As we said, two different bosonic Hamiltonians could be equivalent if they were related by canonical transformations/renormalizations of variables α and π. This insensitivity simply says that the GDM formalism knows these renormalizations and does them correctly. In model 1 we also find this insensitivity (not shown). Finally we notice that in regions of $\omega^2 \sim 1/\Omega$, calculations that go to higher orders in EOM may give unphysical results. This is again because the EOMs are accurate only in the leading order of $1/\Omega$. The fact that this "divergence" appears slightly before

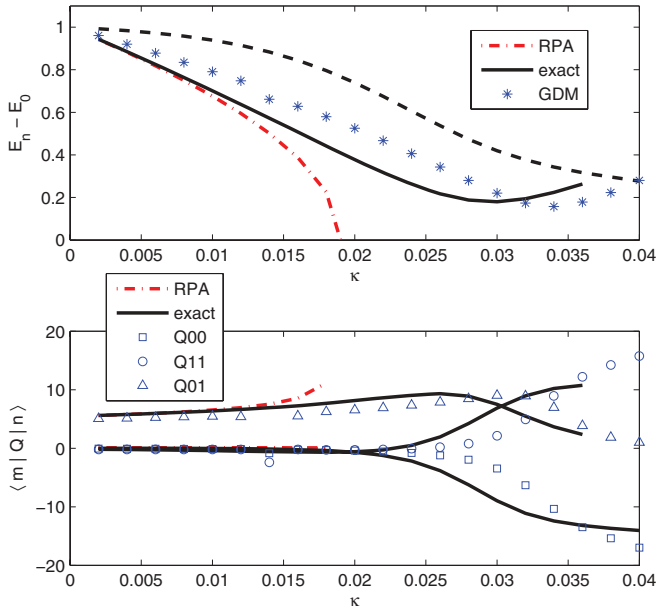

FIG. 5. (Color online) Excitation energies $E_n - E_0$ and transition matrix elements $\langle m|Q|n\rangle$ in model 4 as a function of κ. The black solid lines are exact results of shell-model diagonalization. The black dashed line is the beginning of the single-particle continuum. The red dashed-dotted lines are the RPA results. The blue symbols are the GDM results. The stars are energies; the squares, circles, and up triangles are matrix elements of Q between different states.

the instability point of RPA shown in Fig. 3 indicates again that the correct ω^2 may be smaller than the one calculated by RPA.

Models 3 and 4. At last we consider two models with s.p. configurations that are asymmetric in upper and lower groups, which generates odd anharmonicities that are necessary for deformation. In model 3, the lower group has 10 s.p. levels with $m = \pm\frac{3}{2}, \ldots, \pm\frac{11}{2}$, and the upper group has 14 s.p. levels with $m = \pm\frac{1}{2}, \ldots, \pm\frac{13}{2}$. In model 4, the lower group has 12 s.p. levels with $m = \pm\frac{1}{2}, \ldots, \pm\frac{11}{2}$, and the upper group has 10 s.p. levels with $m = \pm\frac{1}{2}, \ldots, \pm\frac{9}{2}$. In both models, operator q still has the selection rule of $\Delta m = 0, \pm 1$, with nonvanishing matrix elements set to be 1. Model 3 has a slightly larger asymmetry than that of model 4, and their signs of the asymmetry are different.

These two models are more complicated in the sense that now there are more active degrees of freedom (odd anharmonicities). In the GDM method, possibly the simplest calculation is done. We keep in H_b only $\Lambda^{(30)}$, $\Lambda^{(12)}$, and $\Lambda^{(40)}$ (besides $\omega^2\alpha^2/2$ and $\pi^2/2$). $\Lambda^{(30)}$ and $\Lambda^{(12)}$ are fixed by requiring $Q^{(20)} = Q^{(02)} = 0$ in the solution (4). Then $\Lambda^{(40)}$ is fixed by the constraint from the fourth order in EOM. The requirement $Q^{(20)} = Q^{(02)} = 0$ is the same as that for models 1 and 2 without upper-lower asymmetry, by which $\Lambda^{(30)}$ and $\Lambda^{(12)}$ vanish.

The results are shown in Figs. 4 and 5. The deformation begins around the critical point of RPA when ω^2 becomes negative. In the vibrational region the potential is stiff and deformation is not easy. As κ increases, the potential becomes flat on the bottom and finally has a double-well shape. Then, even a relatively small odd anharmonicity (here mainly $\Lambda^{(30)}$) can tilt the potential and generate large deformation. We notice first that the GDM calculations give the correct sign of deformations: positive and negative for the ground and first-excited state of model 3, and vice versa for model 4. In realistic situation $\Lambda^{(30)}[(\hat{\alpha}\times\hat{\alpha})^2\times\hat{\alpha}]^0 \sim \Lambda^{(30)}\beta^3\cos 3\gamma$ ($\hat{\alpha}$ is the quadrupole phonon and β, γ are Bohr angles), the sign of $\Lambda^{(30)}$ "determines" the intrinsic shape of the nucleus (prolate or oblate). This is especially interesting in the transitional regions, where the rotor formula is not applicable. Second, the quantitative agreement of deformation is also good except at the largest κ. There the deformation "saturates" toward its maximal possible value within the model space, favored by energy. Meanwhile in the boson mapping, we are too close to the boundary of the finite physical bosonic space, and the GDM results become inaccurate. In realistic nuclei this "saturation" may not happen. The number of participating and active nucleons is usually around 30 in well-deformed nuclei, which is much larger than the number (typically 10) in the current models. Finally, we point out that the first-excited state in our simple models is not a "rotational" state; rather it corresponds to the next "band head" in realistic rotational nuclei. The rotational states that are very low in energy come in only in three dimensions.

III. CONCLUSION

In this work we demonstrate the validity of the GDM procedure for microscopic calculation of the collective/bosonic Hamiltonian. The lowest several states of this bosonic Hamiltonian reproduce quite well the collective states of the exact shell model, both for energies and transition rates, in a wide range from vibrational, γ-unstable, to deformed systems. Specifically, we show that deformation can be described without introducing a deformed mean field. The traditional procedure of "symmetry breaking and restoration," first "statically" breaks rotational symmetry in the ground state by representing the latter as a Slater determinant of deformed s.p. levels (Nilsson levels) and then projects afterward to good angular momentum. However, in the case of large shape fluctuations (flat minimum of energy surface) or shape coexistence (two close minima), it may fail. On the other hand, the GDM procedure always conserves the rotational symmetry. Deformations are put in "dynamically" at higher orders (for example, cubic terms) beyond the mean field. Thus it is suitable to describe such phenomena as shape fluctuations and coexistence.

In realistic nuclei, the gap of s.p. continuum is generated by the pairing correlations. The GDM formalism based on the Hartree-Fock-Bogoliubov variational method is straightforward as shown in Ref. [9]. However, another treatment may be possible. Instead of introducing Bogoliubov quasiparticles and representing the ground state as their vacuum, the pairing correlations are considered in higher orders beyond the mean field, by keeping both the particle-hole and particle-particle channels in the factorization $a_4^\dagger a_3^\dagger a_2 a_1 \approx a_4^\dagger a_1 \cdot a_3^\dagger a_2 - a_4^\dagger a_2 \cdot a_3^\dagger a_1 + a_4^\dagger a_3^\dagger \cdot a_2 a_1$. In this way the exact particle number is always conserved. Work along this line is in progress, and

results seem promising. We are also generalizing the GDM code by including angular-momentum vector coupling that is necessary for realistic calculations.

ACKNOWLEDGMENT

This work was supported by the NSF Grants No. PHY-0758099 and No. PHY-1068217.

[1] A. Bohr and B. Mottelson, *Nuclear Structure* (Benjamin, New York, 1975), Vol. 2.
[2] L. Prochniak and S. G. Rohozinski, J. Phys. G: Nucl. Part. Phys. **36**, 123101 (2009).
[3] A. Arima and F. Iachello, Ann. Rev. Nucl. Part. Sci. **31**, 75 (1981); F. Iachello and A. Arima, *The Interacting Boson Model* (Cambridge University Press, Cambridge, 1987).
[4] L. Y. Jia and V. G. Zelevinsky, Phys. Rev. C **84**, 064311 (2011).
[5] A. Kerman and A. Klein, Phys. Rev. **132**, 1326 (1963).
[6] S. T. Belyaev and V. G. Zelevinsky, Yad. Fiz. **11**, 741 (1970) [Sov. J. Nucl. Phys. **11**, 416 (1970)]; Yad. Fiz. **16**, 1195 (1972) [Sov. J. Nucl. Phys. **16**, 657 (1973)]; Yad. Fiz. **17**, 525 (1973) [Sov. J. Nucl. Phys. **17**, 269 (1973)].
[7] V. G. Zelevinsky, Prog. Theor. Phys. Suppl. **74–75**, 251 (1983).
[8] M. I. Shtokman, Yad. Fiz. **22**, 479 (1975) [Sov. J. Nucl. Phys. **22**, 247 (1976)].
[9] L. Y. Jia, Phys. Rev. C **84**, 024318 (2011).